Next-to-leading order QCD corrections to $W^+W^-\gamma$ and $ZZ\gamma$ production with leptonic decays

G. Bozzi,[1] F. Campanario,[2,3] V. Hankele,[2] and D. Zeppenfeld[2]

[1]*Dipartimento di Fisica, Università di Milano and INFN, Sezione di Milano Via Celoria 16, I-20133 Milano, Italy*
[2]*Institut für Theoretische Physik, Karlsruhe Institute of Technology, Universität Karlsruhe, 76128 Karlsruhe, Germany*
[3]*Departament de Física Teòrica and IFIC, Universitat de València-CSIC, E-46100, Burjassot, València, Spain*

The computation of the $\mathcal{O}(\alpha_s)$ QCD corrections to the cross sections for $W^+W^-\gamma$ and $ZZ\gamma$ production in hadronic collisions is presented. We consider the case of a real photon in the final state, but include full leptonic decays of the W and Z bosons. Numerical results for the LHC and the Tevatron are obtained through a fully flexible parton level Monte Carlo program based on the structure of the VBFNLO program, allowing an easy implementation of arbitrary cuts and distributions. We show the dependence on scale variations of the integrated cross sections and provide evidence that next-to-leading order (NLO) QCD corrections strongly modify the LO predictions for observables at the LHC both in magnitude and in shape.

PACS numbers: 12.38.Bx, 13.85.−t, 14.70.−e, 14.70.Bh

I. INTRODUCTION

The experimental precision that will be reached in cross section measurements at the CERN Large Hadron Collider (LHC) demands an effort of the theoretical community in providing accurate phenomenological predictions. Next-to-leading order (NLO) QCD corrections for cross sections and distributions have thus become mandatory, and many relevant processes at hadron colliders are now known to this accuracy.

Events with multiple gauge bosons in the final state provide an irreducible background to many new physics searches (see, for instance, [1] for a discussion of the relevant backgrounds in the search of new physics at the LHC). In addition, the triple gauge couplings involved in the contributing diagrams allow for restrictive tests of the gauge sector of the standard model. The process $pp \rightarrow W^+W^-\gamma + X$ is particularly important since it is also sensitive to four gauge boson couplings, namely, the $WWZ\gamma$ and $WW\gamma\gamma$ vertices [2]. Given the small cross sections involved, such a measurement will require very high luminosity running as may become available with an upgrade of the LHC machine.

In this paper, we present the $\mathcal{O}(\alpha_s)$ corrections for the processes

"$W^+W^-\gamma$": $pp, p\bar{p} \rightarrow \nu_{l_1} l_1^+ \bar{\nu}_{l_2} l_2^- \gamma + X,$

"$ZZ\gamma$": $pp, p\bar{p} \rightarrow l_1^+ l_1^- l_2^+ l_2^- \gamma + X.$ (1.1)

Similar to previous work on triple weak boson production [3–6], we find that the QCD corrections are sizable and also modify the shape of the differential distributions for many observables: this proves that a simple rescaling of the LO results is not adequate and a full NLO Monte Carlo program is needed for a quantitative determination of quartic couplings at the LHC. We have implemented our calculation within the vector boson fusion and more at next-to-leading order (VBFNLO) framework [7], a fully flexible parton level Monte Carlo program, which allows the definition of arbitrary acceptance cuts and distributions.

The paper is organized as follows: in Sec. II we provide an example of the relevant Feynman diagrams at tree level, a short account of the strategies used to compute the real and virtual corrections, and the various checks performed both internally and against other available codes. In Sec. III we show numerical results, including the scale variations of the LO and NLO integrated cross sections and some selected differential distributions. Conclusions are given in Sec. IV.

II. THE CALCULATION

We consider the processes (1.1) up to order $\alpha_s\alpha^6$ in the limit where all fermions are massless. Among the LO diagrams (110 in the "$W^+W^-\gamma$" case, 336 in the "$ZZ\gamma$" case) we can distinguish three different topologies: they correspond to the cases when 1, 2, or 3 vector bosons are attached to the quark line. [These are, respectively, cases (a), (b), or (c) of Fig. 1, where examples for $W^+W^-\gamma$ production are shown. The single and double vertex topologies of Figs. 1(a) and 1(b) also exist for $ZZ\gamma$ production since we include off-shell effects in our
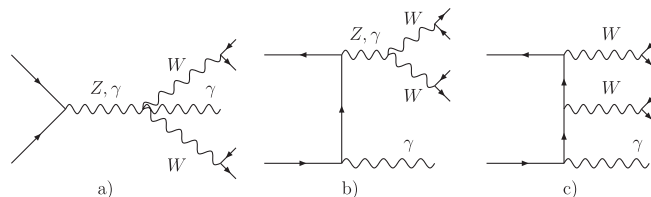

FIG. 1. Examples of the three topologies of Feynman diagrams contributing to the process $pp \rightarrow W^+W^-\gamma + X$ at tree level.

calculation; i.e. the photon or a Z boson can be radiated off a final state lepton.]

In all cases, the leptonic decays of the W and Z bosons and combinations of subgraphs corresponding to decays of the same virtual W, Z, or photon are factorized in the form of *leptonic tensors* and computed independently from the rest of the cross section, in analogy with the procedure in [8]: this reduces computational time since the same decay current may appear in many Feynman diagrams and in different subprocesses and can, thus, be computed once for each phase-space point and saved for later use. For the computation of the matrix elements, we use the helicity method introduced in [9].

The cross section at order α_s contains contributions from real emission and virtual corrections from the interference of one-loop diagrams with the Born amplitude. We use the Catani-Seymour dipole subtraction method [10] to handle the cancellation of infrared divergences between real emission and virtual corrections. Factorization of initial state collinear singularities into the parton distribution functions leads to additional "finite collinear terms."

The NLO real corrections are generated by the emission of a gluon off the quark line or by the emission of a quark through a $g \to q\bar{q}$ splitting in the initial state. The strategy of computing *leptonic tensors* separately proves to be particularly useful in this case, since we have a total of 272 (896) different Feynman diagrams contributing to the $W^+W^-\gamma$ ($ZZ\gamma$) process when attaching an additional gluon to the Born diagrams.

In the case of real emissions, the definition of an isolated on-shell photon requires further discussion. Photon emission collinear to a massless quark results in an additional singularity, which needs to be regularized. The simple rejection of events containing partons inside a cone of fixed width drawn around the photon is not a permissible choice since it will suppress the phase space for soft gluon emissions and spoil the cancellation of infrared divergences. In this paper we avoid the complications of quark fragmentation to photons by using an effective method that has been proposed by Frixione [11]. The precise definition of this *photon isolation cut* is discussed in Sec. III.

The NLO virtual corrections come from the interference of leading order diagrams with one-loop diagrams obtained by attaching a gluon to the quark-antiquark line. In the case where only one vector boson is attached to the quark line, i.e. topology (a), one only has vertex corrections, while diagrams belonging to topologies (b) and (c) give rise to boxes and pentagons. The tensor coefficients of the loop integrals have been computed à la Passarino-Veltman [12] up to box level, while the Denner-Dittmaier reduction procedure [13] has been used for the pentagons, which avoids the problem of small Gram determinants occurring in pentagons with planar configurations of the external momenta. Denner-Dittmaier reduction is now fully imple-

mented in the public version of the VBFNLO code. The overall contribution from virtual corrections can be written as

$$M_V = \tilde{M}_V + \frac{\alpha_S}{4\pi}C_F\left(\frac{4\pi\mu^2}{Q^2}\right)^\epsilon\Gamma(1 + \epsilon)$$
$$\times\left[-\frac{2}{\epsilon^2} - \frac{3}{\epsilon} - 8 + \frac{4\pi^2}{3}\right]M_B, \qquad (2.1)$$

where M_B is the Born amplitude and Q is the partonic center-of-mass energy, i.e. the invariant mass of the final state $VV\gamma$ system. The term $\tilde{M}_V$ is the finite part of the virtual corrections to 2 and 3 weak boson amplitudes as in Figs. 1(b) and 1(c), which we call boxline and pentline contributions in the following, so named since boxes and pentagons constitute the most complex loop diagrams, respectively.

We have verified analytically and numerically that in order to obtain the above factorization formula of the infrared divergences against the born amplitude, the transversality property of the photon [$\epsilon(p_\gamma) \cdot p_\gamma = 0$] must be used; otherwise, additional IR singularities that are not proportional to the born amplitude do appear. After checking that there are no additional $1/\epsilon$ terms due to the massless on-shell photon, the analytical structure of $\tilde{M}_V$ can be obtained from the massive weak boson case considered in [5]. Nevertheless, we have recomputed equivalent pentline and boxline contributions for massless particles and found that they agree at the double precision accuracy level with those of [5], once the proper scalar integrals are used.

A further reduction of computing time is obtained for $W^+W^-\gamma$ production by implementing a trick already used in [4,5,8]. We write the polarization vector of the vector bosons as

$$\epsilon_V^\mu = x_V q_V^\mu + \tilde{\epsilon}_V^\mu, \qquad (2.2)$$

where q_V is the momentum of the massive boson ($V = W^\pm$). A pentagon contracted with one of the external momenta q_V can always be reduced to a difference of box diagrams. Thus we effectively isolate a *true* pentagon contribution and shift the rest of the 5-point contribution to the less time-consuming boxes. The remainder $\tilde{\epsilon}_V$ is chosen in such a way that

$$\tilde{\epsilon}_V \cdot (q_{V_1} + q_{V_2}) = 0; \qquad (2.3)$$

i.e., the time component of the shifted polarization vector is zero in the center-of-mass system of the V pair. This choice yields particularly small pentline contributions, which, hence, can be determined with lower Monte Carlo statistics. For $ZZ\gamma$ production, the pentline contributions group into gauge invariant subsets, which are invariant under the replacement of Eq. (2.2). Thus the trick does not speed up the code but provides a consistency check for the calculation.

We have performed a number of checks on our final results. First, we compared all tree-level matrix elements (including the ones for real emission corrections) against amplitudes generated by `MadGraph` [14]: the agreement is at the level of machine precision (10^{-15}). Second, we have compared the LO cross sections for both $pp \rightarrow W^+W^-\gamma + X$ and $pp \rightarrow ZZ\gamma + X$ against `HELAC` [15] and found agreement at the per mill level. Third, we have compared integrated tree-level cross sections for $pp(p\bar{p}) \rightarrow W^+W^-\gamma(j) + X$ and $pp(p\bar{p}) \rightarrow ZZ\gamma(j) + X$ against `MadEvent` and `Sherpa` [16], finding agreement at the per mill level. Finally, we also performed gauge tests based on Ward identities for the NLO virtual corrections at different levels of complexity.

III. RESULTS

Numerical results have been obtained through the implementation of our calculation into a NLO Monte Carlo program based on the structure of the `VBFNLO` code [7]. This and other processes with a real photon in the final state will be included in the public version of `VBFNLO` in a future release.

The value of the total cross section for $ZZ\gamma$ production, including leptonic Z decays, turns out to be less than a femtobarn at LHC energies: since it will probably be too hard to detect, at least in an early luminosity run, in this section we focus on the $pp \rightarrow W^+W^-\gamma + X$ process.

For the electroweak parameters we use the W and Z boson masses and the Fermi constant as input. From these we derive the electromagnetic coupling and the weak mixing angle via tree-level relations, i.e; we use

$$m_W = 80.398 \text{ GeV}, \qquad \sin^2(\theta_W) = 0.222\,64,$$
$$G_F = 1.16637 \cdot 10^{-5} \text{ GeV}^{-2}, \qquad \alpha^{-1} = 132.3407.$$
$$(3.1)$$

We do not consider bottom and top quark effects. The remaining quarks are assumed to be massless, and we work in the approximation where the Cabibbo-Kobayashi-Maskawa matrix is the identity matrix. We choose the invariant $W^+W^-\gamma$ mass as the central value for the factorization and renormalization scales:

$$\mu_F = \mu_R = \mu_0 = \sqrt{(p_{\ell_1} + p_{\ell_2} + p_{\nu_1} + p_{\nu_2} + p_\gamma)^2}.$$
$$(3.2)$$

We use the CTEQ6L1 parton distribution function at LO and the CTEQ6M set with $\alpha_S(m_Z) = 0.1176$ at NLO [17].

Since the photon can be emitted either from the initial quark line or from each of the two final state charged leptons, we divide the phase space into three separate regions in which we use different mappings of random numbers on phase-space variables, designed for optimal Monte Carlo convergence for the dominating Feynman graphs. The regions are generated as (approximately) on-

shell $W^+ \rightarrow e^+\nu_e\gamma$ and $W^- \rightarrow \mu^-\bar{\nu}_\mu\gamma$ three-body decay and triple electroweak boson production, respectively, and are chosen according to whether $m(e^+\nu_e\gamma)$ or $m(e^-\bar{\nu}_e\gamma)$ is closest to M_W or whether both are sufficiently off resonance. We impose a set of minimal cuts on the rapidity, $y_{\gamma(\ell)}$, and the transverse momenta, $p_{T_{\gamma(\ell)}}$, of the photon and the charged leptons, which are designed to represent typical experimental requirements. Furthermore, leptons, photons, and jets must be well separated in the rapidity-azimuthal angle plane. Specifically, the cuts we impose are

$$p_{T_{\gamma(\ell)}} > 20 \text{ GeV}, \qquad |y_{\gamma(\ell)}| < 2.5, \qquad R_{\ell\gamma} > 0.4,$$
$$R_{j\ell} > 0.4, \qquad R_{j\gamma} > 0.7, \qquad (3.3)$$

where, in our simulations, a jet is defined as a colored parton of transverse momentum $p_{Tj} > 20$ GeV. For photon isolation, we implement the procedure introduced in [11]: if i is a parton with transverse energy E_{T_i} and a separation $R_{i\gamma}$ with a photon of transverse momentum p_{T_γ}, then the event is accepted only if

$$\Sigma_i E_{T_i} \theta(\delta - R_{i\gamma}) \leq p_{T_\gamma} \frac{1 - \cos\delta}{1 - \cos\delta_0} \qquad \text{(for all } \delta \leq \delta_0\text{)},$$
$$(3.4)$$

where δ_0 is a fixed separation that we set equal to 0.7. A quick look at Eq. (3.4) reveals that a sufficiently soft gluon can be arbitrarily close to the photon axis, while the energy of an exactly collinear parton must be vanishing in order to pass the isolation cut. Collinear-only events (leading to fragmentation contributions) are thus rejected, while soft emissions are retained, as desired. Additionally, for $ZZ\gamma$ production we impose that the invariant mass of any combination of two opposite-charged leptons, $m_{\ell\ell}$, be larger than 15 GeV in order to avoid virtual-photon singularities in $\gamma^* \rightarrow l^+l^-$ at a low $m_{\ell\ell}$. In Table I, we give results for the integrated cross sections for $W^+W^-\gamma$ and $ZZ\gamma$ production at the LHC for the given cuts as well as for a harder cut on the photon transverse momentum of $p_{T_\gamma} > 30$ GeV. In Table II, the numbers for the Tevatron are presented for the cuts as in Eqs. (3.3) and (3.4), but for less restrictive transverse-momentum cuts, $p_{T_{\gamma(\ell)}} > 10(10)$ GeV and $p_{T_{\gamma(\ell)}} > 20(10)$ GeV. The center-of-mass energy is set to 14 TeV for the LHC and 1.96 TeV for Tevatron collisions, respectively.

In the following we show $W^+W^-\gamma$ results for the process $pp \rightarrow \nu_e e^+ \bar{\nu}_\mu \mu^- \gamma + X$; i.e. we do not consider interference effects due to identical leptons. At LO, interference terms contribute 0.1% or less to the total cross section and are, thus, negligible. The cross sections have been multiplied by a combinatorial factor of 4, however, and correspond to the production of any combination of electrons or muons.

In order to estimate the scale uncertainty of the total cross section, we study the variation of the numerical

TABLE I.   Total cross sections at the LHC for $pp \to W^+W^-\gamma + X$ and $pp \to ZZ\gamma + X$ with leptonic decays, at LO and NLO, and for two sets of cuts. Relative statistical errors of the Monte Carlo program are below 10^{-3}.

LHC	LO [fb]	NLO [fb]
$\sigma(\text{"}WW\gamma\text{"} \to e^+\nu\mu^-\bar{\nu}\gamma)\ p_{T_{\gamma(\ell)}} > 20(20)\ \text{GeV}$	1.695	2.881
$\sigma(\text{"}WW\gamma\text{"} \to e^+\nu\mu^-\bar{\nu}\gamma)\ p_{T_{\gamma(\ell)}} > 30(20)\ \text{GeV}$	0.9580	1.738
$\sigma(\text{"}ZZ\gamma\text{"} \to e^+e^-\mu^+\mu^-\gamma)\ p_{T_{\gamma(\ell)}} > 20(20)\ \text{GeV}$	0.077 86	0.1062
$\sigma(\text{"}ZZ\gamma\text{"} \to e^+e^-\mu^+\mu^-\gamma)\ p_{T_{\gamma(\ell)}} > 30(20)\ \text{GeV}$	0.039 69	0.055 77

TABLE II.   Total cross sections at the Tevatron for $p\bar{p} \to W^+W^-\gamma + X$ and $p\bar{p} \to ZZ\gamma + X$ with leptonic decays, at LO and NLO, and for two sets of cuts. Relative statistical errors of the Monte Carlo program are below 10^{-3}.

Tevatron	LO [fb]	NLO [fb]
$\sigma(\text{"}WW\gamma\text{"} \to e^+\nu\mu^-\bar{\nu}\gamma)\ p_{T_{\gamma(\ell)}} > 10(10)\ \text{GeV}$	0.9015	1.271
$\sigma(\text{"}WW\gamma\text{"} \to e^+\nu\mu^-\bar{\nu}\gamma)\ p_{T_{\gamma(\ell)}} > 20(10)\ \text{GeV}$	0.3755	0.5342
$\sigma(\text{"}ZZ\gamma\text{"} \to e^+e^-\mu^+\mu^-\gamma)\ p_{T_{\gamma(\ell)}} > 10(10)\ \text{GeV}$	0.054 69	0.076 81
$\sigma(\text{"}ZZ\gamma\text{"} \to e^+e^-\mu^+\mu^-\gamma)\ p_{T_{\gamma(\ell)}} > 20(10)\ \text{GeV}$	0.024 40	0.034 41

results in the interval

$$\mu_F, \qquad \mu_R = \xi \cdot \mu_0 \qquad (0.1 < \xi < 10), \qquad (3.5)$$

where μ_0 is the $W^+W^-\gamma$ or $ZZ\gamma$ invariant mass. The variation of the total $W^+W^-\gamma$ cross section at LO and NLO is shown on the left panel of Fig. 2. It is evident that the LO scale variation greatly underestimates the size of NLO corrections, which give a K-factor of 1.70 for $\mu_F = \mu_R = \mu_0$. The NLO scale uncertainty is about 6% when varying the factorization and the renormalization scale $\mu = \mu_F = \mu_R$ up and down by a factor of 2 around the reference scale $\mu_0 = Q$, slightly smaller than for the LO

uncertainty, and it is dominated by the dependence on μ_R, which gives a negative slope with increasing energy, while it has a quite flat dependence on μ_F.

On the right panel of Fig. 2, the scale dependence and relative size of the different NLO contributions are shown. One clearly sees that almost the entire scale variation of the integrated NLO cross section is accounted for by the real emission contributions, defined here as the real emission cross section minus the Catani-Seymour subtraction terms plus the finite collinear terms. The virtual contributions proportional to the Born matrix element [due to the M_B term in Eq. (2.1)] constitute the bulk of the NLO correc-
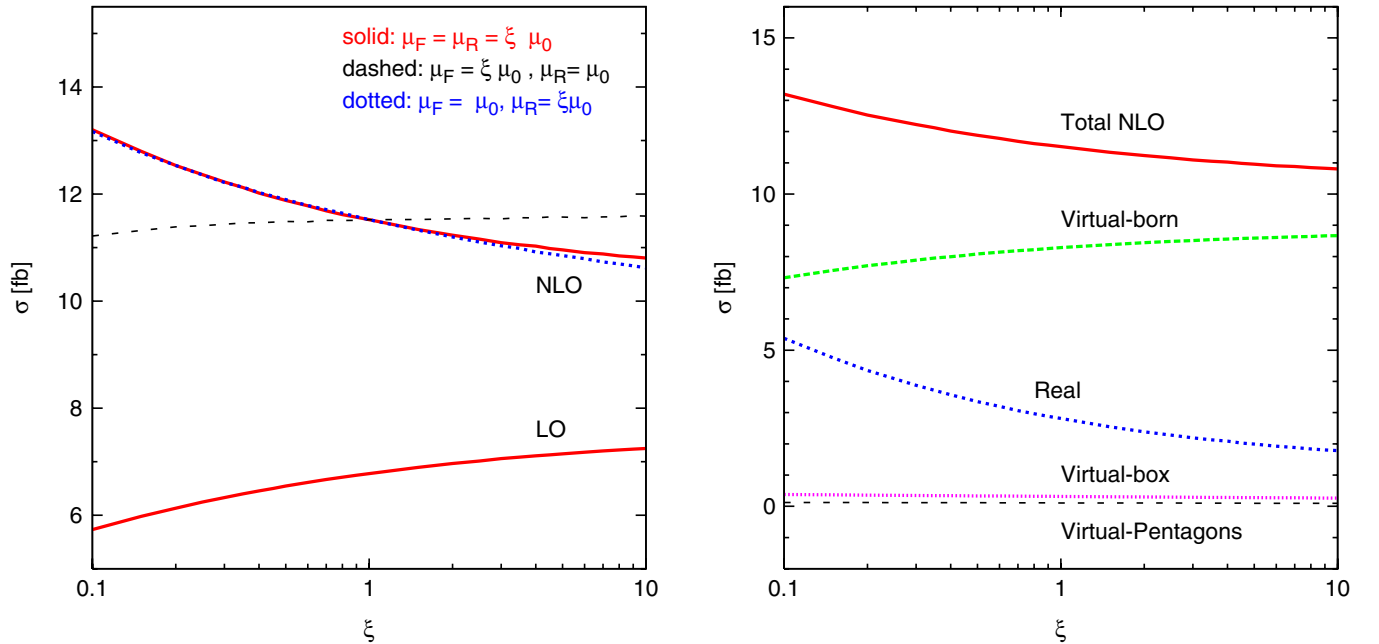

FIG. 2 (color online).   Left: Scale dependence of the total LHC cross section for $pp \to W^+W^-\gamma + X \to \ell^+\ell^-\gamma + \not{p}_T + X$ at LO and NLO within the cuts of Eqs. (3.3) and (3.4). The factorization and renormalization scales are together or independently varied in the range from $0.1 \cdot \mu_0$ to $10 \cdot \mu_0$. Right: Same as in the left panel but for the different NLO contributions at $\mu_F = \mu_R = \xi\mu_0$.
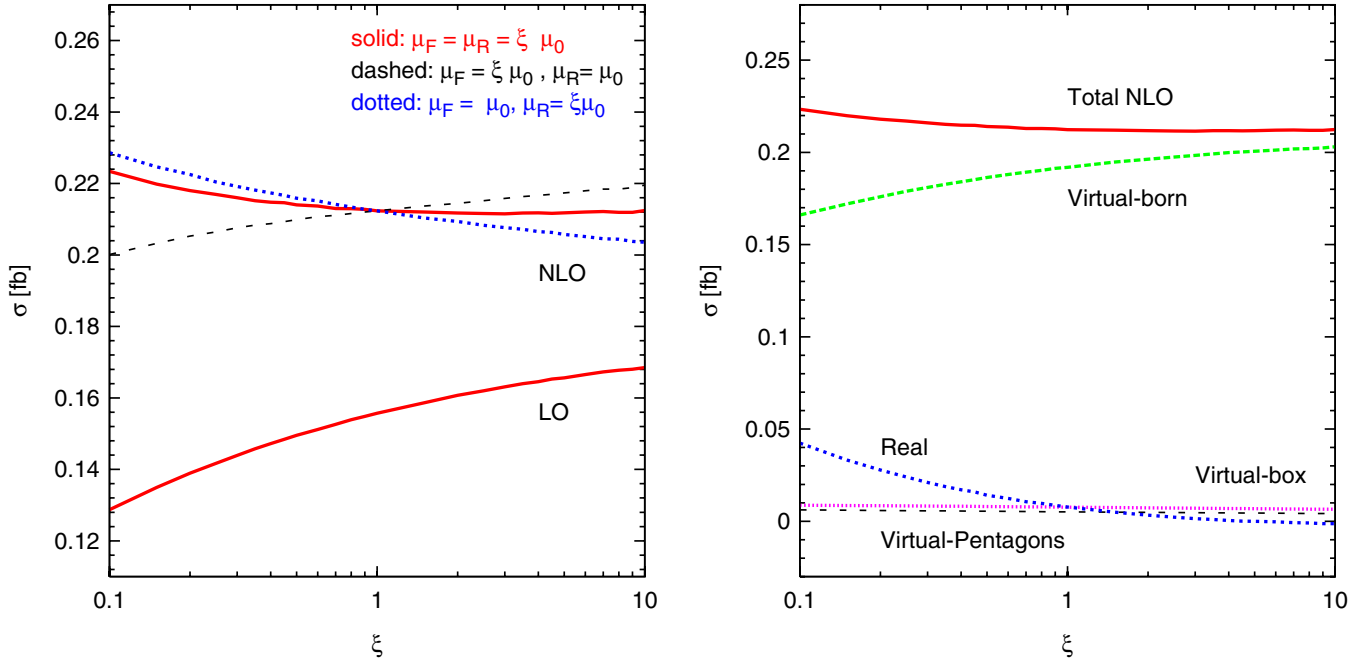
FIG. 3 (color online).   Left: Scale dependence of the total LHC cross section for $pp \to ZZ\gamma + X \to \ell_1^+ \ell_1^- \ell_2^+ \ell_2^- \gamma + X$ at LO and NLO within the cuts of Eqs. (3.3) and (3.4). The factorization and renormalization scales are together or independently varied in the range from $0.1 \cdot \mu_0$ to $10 \cdot \mu_0$. Right: Same as in the left panel but for the different NLO contributions at $\mu_F = \mu_R = \xi \mu_0$.

tions, being roughly twice as large as the real emissions, while the finite virtual remainders due to boxes and pentagons represent only 3% and less than 1% of the total result, respectively, and their scale dependence is basically flat.

Similar considerations apply for $ZZ\gamma$ production where a combinatorial factor of 2 has been included for $pp \to ZZ\gamma + X \to \ell_1^+ \ell_1^- \ell_2^+ \ell_2^- \gamma + X$. In Fig. 3, one observes that the overall scale variation decreases when varying the factorization and the renormalization scale
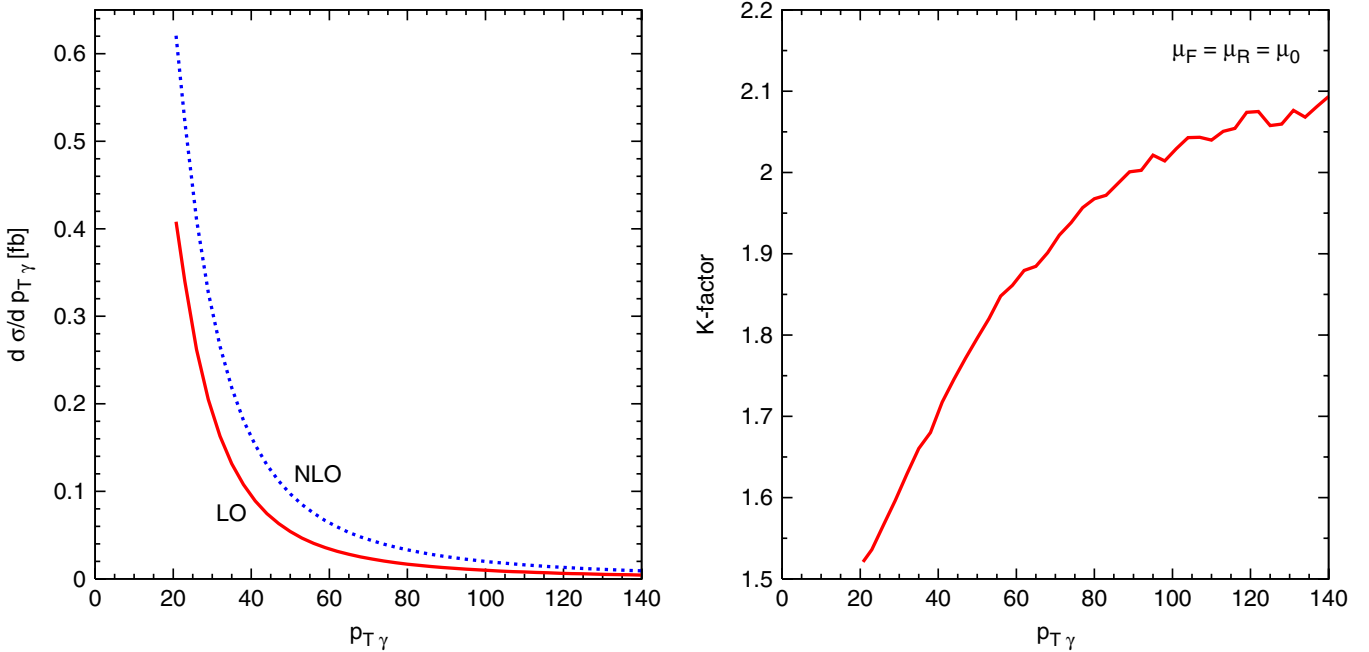

FIG. 4 (color online).   Left: Transverse-momentum distribution of the photon in $W^+ W^- \gamma$ production at the LHC. LO and NLO results are shown for $\mu_F = \mu_R = \mu_0$ and the cuts of Eq. (3.3). Right: K-factor for the transverse-momentum distribution of the photon as defined in Eq. (3.6).
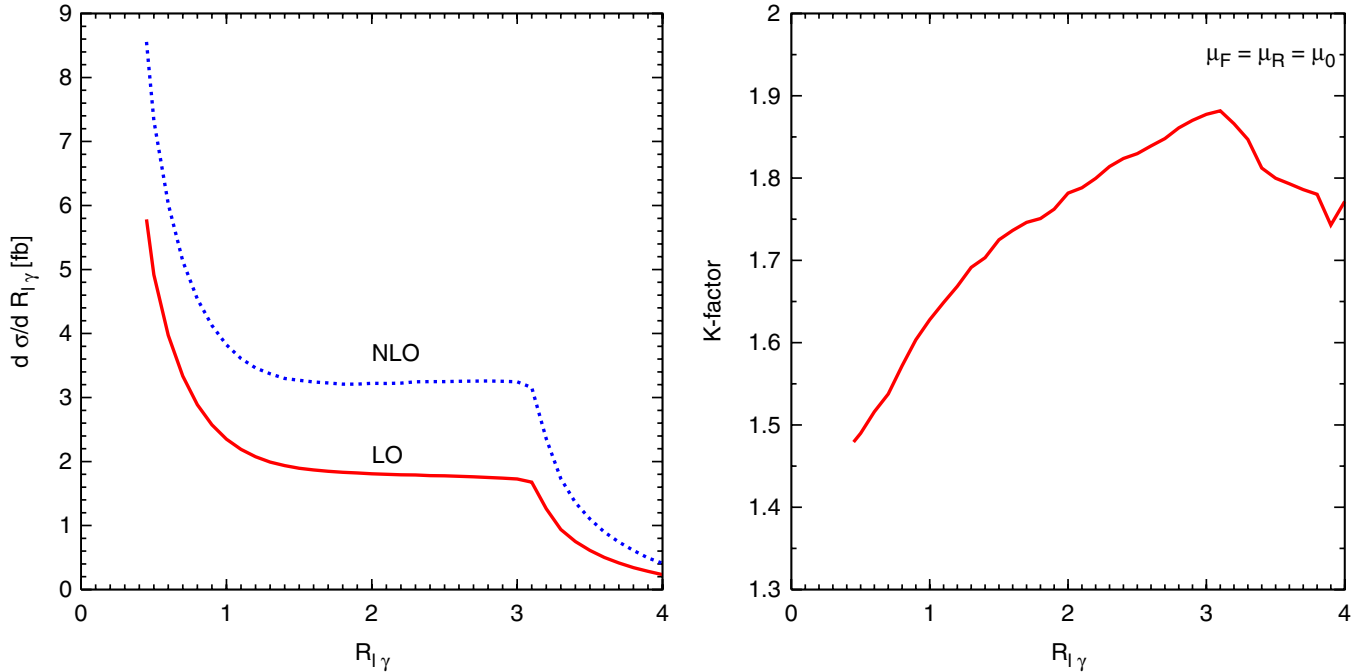
FIG. 5 (color online).   Left: Separation between the photon and the softest lepton in $W^+W^-\gamma$ production at the LHC, at LO and NLO with $\mu_F = \mu_R = \mu_0$ and the cuts of Eq. (3.3). Right: K-factor for the separation between the photon and the softest lepton as defined in Eq. (3.6).

$\mu = \mu_R = \mu_0$ up and down by a factor of 2 around the reference scale $\mu_0 = Q$ from roughly $\pm 7\%$ at LO to $\pm 1\%$ at NLO, and we have a K-factor of 1.36 for $\mu_F = \mu_R = \mu_0$. The main difference with respect to the $W^+W^-\gamma$ case is the numerical contribution of the real corrections, which amounts to 20% of the total contribution or less.

The NLO contributions cannot be described by a simple rescaling of the LO results since the corrections show a strong dependence on the phase-space region under investigation. As practical examples, we plot two differential distributions at LO and NLO together with the associated K-factor, defined as

$$K = \frac{d\sigma^{\text{NLO}}/dx}{d\sigma^{\text{LO}}/dx}. \qquad (3.6)$$

The observables x considered are the transverse momentum of the photon and the separation between the softest (lowest-p_T) lepton and the photon in $W^+W^-\gamma$ production at the LHC. In Fig. 4 we show the transverse-momentum distribution of the on-shell photon: the corresponding K-factor increases from 1.5 at $p_{T\gamma} = 20$ GeV to 2.1 at $p_{T\gamma} = 140$ GeV. In Fig. 5, we consider the separation between the photon and the softest lepton, and a similar variation of the K-factor in the range 1.5–1.9 is observed.

IV. CONCLUSIONS

We have calculated the NLO QCD corrections to the processes pp, $p\bar{p} \rightarrow W^+W^-\gamma + X$ and pp, $p\bar{p} \rightarrow ZZ\gamma +$

X with full leptonic decays of the W and Z bosons. These processes can be relevant both for new physics searches (as a background) and for the measurement of quartic gauge couplings (as a signal) at the LHC.

Our numerical results show sizable cross section increases with respect to the LO calculation, ranging from 40% to as much as 100% in certain regions of phase space. $W^+W^-\gamma$ and $ZZ\gamma$ production at the LHC provide additional examples of cross sections whose theoretical errors at LO are substantially underestimated by considering scale variations only: the LO factorization scale variation is much smaller than the NLO correction. Remaining NLO scale variations are at the 10% level (e.g. $\pm 6\%$ for the integrated $W^+W^-\gamma$ production cross section at the LHC when varying $\mu_R = \mu_F = \mu$ by a factor of 2 around the reference scale $\mu = Q = m_{WW\gamma}$).

Given the size of the higher-order corrections and, in particular, their strong dependence on the observable and on different phase-space regions under investigation, a fully exclusive NLO parton Monte Carlo program for $W^+W^-\gamma$ and $ZZ\gamma$ production is required to match the expected precision of the LHC measurements. We plan to incorporate this and other processes with a final state photon into the VBFNLO package in the near future.

---

[1] J. M. Campbell, J. W. Huston, and W. J. Stirling, Rep. Prog. Phys. **70**, 89 (2007).

[2] S. Godfrey, arXiv:hep-ph/9505252; P. J. Dervan, A. Signer, W. J. Stirling, and A. Werthenbach, J. Phys. G **26**, 607 (2000); O. J. P. Eboli, M. C. Gonzalez-Garcia, S. M. Lietti, and S. F. Novaes, Phys. Rev. D **63**, 075008 (2001); sP. J. Bell, Eur. Phys. J. C **64**, 25 (2009).

[3] A. Lazopoulos, K. Melnikov, and F. Petriello, Phys. Rev. D **76**, 014001 (2007).

[4] V. Hankele and D. Zeppenfeld, Phys. Lett. B **661**, 103 (2008).

[5] F. Campanario, V. Hankele, C. Oleari, S. Prestel, and D. Zeppenfeld, Phys. Rev. D **78**, 094012 (2008).

[6] T. Binoth, G. Ossola, C. G. Papadopoulos, and R. Pittau, J. High Energy Phys. 06 (2008) 082.

[7] K. Arnold *et al.*, Comput. Phys. Commun. **180**, 1661 (2009).

[8] B. Jager, C. Oleari, and D. Zeppenfeld, J. High Energy Phys. 07 (2006) 015; Phys. Rev. D **73**, 113006 (2006); G. Bozzi, B. Jager, C. Oleari, and D. Zeppenfeld, Phys. Rev. D **75**, 073004 (2007).

[9] K. Hagiwara and D. Zeppenfeld, Nucl. Phys. **B274**, 1 (1986); **B313**, 560 (1989).

[10] S. Catani and M. H. Seymour, Nucl. Phys. **B485**, 291 (1997); **B510**, 503 (1998).

[11] S. Frixione, Phys. Lett. B **429**, 369 (1998).

[12] G. Passarino and M. J. G. Veltman, Nucl. Phys. **B160**, 151 (1979).

[13] A. Denner and S. Dittmaier, Nucl. Phys. **B658**, 175 (2003); **734**, 62 (2006).

[14] T. Stelzer and W. F. Long, Comput. Phys. Commun. **81**, 357 (1994); F. Maltoni and T. Stelzer, J. High Energy Phys. 02 (2003) 027.

[15] A. Cafarella, C. G. Papadopoulos, and M. Worek, Comput. Phys. Commun. **180**, 1941 (2009); C. G. Papadopoulos and M. Worek, Eur. Phys. J. C **50**, 843 (2007); A. Kanaki and C. G. Papadopoulos, Comput. Phys. Commun. **132**, 306 (2000).

[16] T. Gleisberg, S. Hoche, F. Krauss, M. Schonherr, S. Schumann, F. Siegert, and J. Winter, J. High Energy Phys. 02 (2009) 007.

[17] J. Pumplin, D. R. Stump, J. Huston, H. L. Lai, P. Nadolsky, and W. K. Tung, J. High Energy Phys. 07 (2002) 012.

[18] J. A. M. Vermaseren, Comput. Phys. Commun. **83**, 45 (1994).